Crossover from low-temperature itinerant to high-temperature localized electron behavior in the electron-doped rare-earth metal cobaltate perovskites

S. L. L. M. Ramos and M. Oguni
Department of Chemistry, Graduate School of Science and Engineering, Tokyo Institute of Technology, 2-12-1 O-okayama, Meguro-ku, Tokyo 152-8551, Japan

Y. Masuda
Department of Environmental Science, Faculty of Science, Niigata University, 2-8050 Ikarashi, Niigata 950-2181, Japan

Y. Inada
Photon Factory, High Energy Accelerator Research Organization (KEK), Tsukuba 305-0801, Japan
(Received 5 October 2010; published 25 February 2011)

We present a study on the temperature dependence of the electronic structure and magnetic properties of $Ce_xEu_{1-x}CoO_3$ by means of x-ray absorption spectroscopy (XAS) and magnetic susceptibility measurements. Contrary to what was previously reported in literature for this compound, we identified the partially substituted Ce species to be tetravalent within the whole temperature range investigated, i.e., $300 \geqslant T/\mathrm{K} \geqslant 40$. It is shown that, as a result, corresponding amounts of Co^{2+} are formed at room temperature, indicating an electron-doping effect. At $T = 40$ K, however, even though electron doping could be identified through Co XAS pre-edge features, the Co^{2+} species were not identifiable. These results indicate a change in the Co-related electronic structure with temperature, and we interpret this as indicative of a crossover from a low-temperature itinerant-electron state to a high-temperature localized-electron state. The magnetic susceptibility revealed the onset of low-temperature itinerant ferromagnetism for the higher Ce-doping concentrations, while the room-temperature effective magnetic moment μ_{eff} value for the lowest Ce-concentrated sample was in complete agreement with the theoretical one for Co^{2+}, thus being consistent with the itinerant–localized-electron crossover scenario as depicted from the XAS results.

DOI: 10.1103/PhysRevB.83.085109 PACS number(s): 71.23.−k, 75.30.Hx, 78.70.Dm

I. INTRODUCTION

The physical properties of solid matter, such as conductivity and magnetism, depend largely on their electronic structure. Within a solid, electrons can be, in principle, described as *itinerant* (collective) or *localized*. In the former case, the electrons are delocalized over the entire solid lattice. The average time that an electron spends near a specific atom, ion, or molecule is very short, and the electrons are spread throughout the lattice with a wavelike nature. Band formalism accounts for the description of such a scenario. On the other hand, in the latter case, the electrons are effectively localized at the atoms in the sense that an electron will spend a relatively long time at a given atom. In this case, the electrons are not distributed in a wavelike organization throughout the lattice, but are rather visualized as particlelike identities, and band formalism fails to account for the description of the system. Large atom-atom interspacing distances or electron correlations (electron-electron interactions) may provide the conditions for stabilizing this localized state.

Contrary to 3*d* transition-metal halides, which invariably host localized electrons, 3*d* transition-metal oxides are known to display either itinerant or localized electron behavior.[1] Prime examples include members of the rare-earth cobaltate perovskite series $RCoO_3$ (R = rare earth), which are known to display a sluggish crossover from localized-electron behavior at low temperatures to itinerant-electron behavior at high temperatures.[2,3] Here, the distinct electronic structures are directly related to the flexibility of the Co ion in the accession to different spin configurations, i.e., low-spin (LS), intermediate-spin (IS), and high-spin (HS) states. This thermally driven spin-state transition involving the Co^{3+} ions from the nonmagnetic LS state to the magnetically active HS (or IS) state has undergone extensive experimental investigations so far, especially in $LaCoO_3$, where the magnetic changes are most pronounced.[3,4] Extension of these studies toward the hole-doped rare-earth cobaltates $A_xR_{1-x}CoO_3$ (A = divalent alkali metal) has contributed to a further understanding of the role of Co^{4+} impurity centers in bringing about changes in the electronic structure. Señarís-Rodríguez and Goodenough[5] have depicted a picture where phase segregation into hole-rich and hole-poor matrixes allows the appearance of complex magnetic interactions as well as the coexistence of itinerant and localized electrons.

In contrast to the large number of investigations dedicated to the electronic structure and physical properties of the hole-doped cobaltates, only slight attention has been paid to the electron-doped counterparts. In theory, partial substitution of the trivalent rare-earth A-site ion R by a tetravalent dopant should yield B-site electron doping. From this point of view, the best candidate for an electron-doped cobaltate perovskite system is $A_xR_{1-x}CoO_3$ (A = Ce, Th). Recently, evidence supporting the electron-doped nature of $A_{0.3}La_{0.7}CoO_{3-\delta}$ (A = Ce, Th) was reported by Pinta *et al.* by means of x-ray absorption spectroscopy (XAS) measurements.[6] They argued that the intensity change of a pre-edge peak correlated with Ce and Th doping indicates the lowering of unoccupied 3*d* density of states, implying that electrons are supplied to the *d* bands;[6] this in turn indicates the existence of Ce^{4+} and

Th^{4+} species. Fuchs *et al.* set about to address the issue of how electron doping affects the magnetic properties of the cobaltates.[7] To this end, they succeeded in preparing thin films of $Ce_xLa_{1-x}CoO_3$ in the composition range $0.1 \leqslant x \leqslant 0.4$ via the pulsed laser deposition method. However, all samples were reported to bear traces of CeO_2 second phase;[7] this problem was also encountered during the preparation of electron-doped manganites.[8] Nevertheless, as predicted previously by the theoretical study of Zhang *et al.*,[9] Fuchs *et al.* found low-temperature ferromagnetism in the entire doping range. The maximum Curie temperature T_c was observed at $x = 0.3$ and the paramagnetic effective moment μ_{eff} increased with Ce doping.[7] The magnetic behavior was understood in terms of an IS ground state $t_{2g}^5 e_g^{1+x}$ when $x > 0.2$ or 0.3, as depicted by a band formalism.

Umemoto *et al.* were the first to have prepared and surveyed the structural and magnetic properties of the solid solution $Ce_xEu_{1-x}CoO_3$ in the range $0 \leqslant x \leqslant 0.15$.[10] Their study focused on a potential valence combination change involving the Eu ions and the Ce dopants. It was demonstrated that the observed temperature dependence of the magnetic susceptibility in the temperature range $5 \leqslant T/\text{K} \leqslant 300$ can be well explained assuming a localized electron scenario with Eu^{3+} and Ce^{3+} and with all the cobalt ions in the trivalent LS state. In this manner, their study suggested a Ce^{3+}-Co^{3+} localized-electron scenario for $Ce_xEu_{1-x}CoO_3$; the scenario differs from the Ce^{4+}-Co^{2+} itinerant-electron one depicted for $Ce_xLa_{1-x}CoO_3$, as suggested from the experimental results by Pinta *et al.*[6] and Fuchs *et al.*[7] and on the band calculation by Zhang *et al.*[9]

In this study, we investigated the valence state of the composing ionic species in $Ce_xEu_{1-x}CoO_3$ by XAS. As explained above, the question whether the valence state of the cerium ion in $Ce_xR_{1-x}CoO_3$ varies as a function of rare-earth element size, i.e., from tetravalent to trivalent as R goes from La (Refs. 6,7, and 9) to Eu,[10] is of great scientific interest. Considering that the attribution of the valence states in $Ce_xEu_{1-x}CoO_3$ by Umemoto *et al.*[10] relied solely on the analysis of the magnetic susceptibility data, we set out to verify their results. The objectives of this study are as follows: (1) to confirm whether the Ce ions are trivalent or tetravalent, (2) to examine the valence state of Co ions, and (3) to elucidate the magnetic behavior of the compound. To this end, we also present our analysis on the magnetic susceptibility.

II. EXPERIMENT

$EuCoO_3$ and $Ce_xEu_{1-x}CoO_3$ ($x = 0.05$, 0.10, 0.15) were prepared by the thermal decomposition of the corresponding cobalticyanide metal complexes $Eu[Co(CN)_6]6H_2O$ and $Ce_xEu_{1-x}[Co(CN)_6]6H_2O$ according to the procedure described previously.[10] Thermal decomposition of metal complexes for the production of perovskite oxides has been reported to yield highly homogeneous samples at relatively low temperatures as compared with other traditional methods, such as the solid-state reaction method and the coprecipitation technique.[11] The samples were characterized by x-ray diffraction (XRD) measurements with a Rigaku Geigerflex RAD-3C using a tube of Cu K_α radiation (wavelength = 1.4518 Å). The refinement of the data was carried out by the Rietveld method using the REITAN 2000 computer program.

$Ce_xEu_{1-x}AlO_3$ ($x = 0$, 0.1) was prepared via a standard solid-state reaction. The starting materials were Eu_2O_3 (Shinetsu Chemical Ltd., 99.9%), $Ce(NO_3)_3$ (Wako Pure Chemical Industries Ltd., 99.9%), and Al_2O_3 (Sigma-Aldrich, 99.9%), and were held in vacuum for several hours before use. The mixture with the stoichiometric composition was ground by ball milling and sintered at 1400 °C for a total of ~40 h with two intermediate grinding treatments, each of 8 h. The XRD profile of $Ce_{0.1}Eu_{0.9}AlO_3$ indicated no traces of impurity and was similar to that of the end-of-composition member $EuAlO_3$, whose successful synthesis was confirmed by matching the XRD profile to a database.

Room-temperature XAS spectra of the powder samples were taken with a Rigaku LOOPER2000 in transmission mode at the Center for Advanced Material Analysis, Tokyo Institute of Technology, with a Ge(220) crystal monochromator. Samples were set between two sheets of adhesive tape. Low-temperature XAS spectra as well as the corresponding room-temperature ones for comparison were taken at BL-12C of the Photon Factory in the High Energy Accelerator Research Organization using a Si(111) double-crystal monochromator. The powders were mixed with boron nitride and pressed into pellets of ~0.5 mm thick. These were fixed between two sheets of adhesive tape. In both experiments, the peak top for the first absorption edges at 5723 eV of the L_3 edge of CeO_2 and at 7709 and 6977 eV of the Co K edge and the Eu L_3 edge of $EuCoO_3$, respectively, were used for energy calibration. The stability of energy at Co K edge is less than ±0.2 eV.[12] All XAS data were analyzed with the program IFEFFIT.[13] Reference samples of $Ce(NO_3)_3$ and CeO_2 were used as purchased. CoO was annealed at 1150 °C overnight and left to cool in N_2 atmosphere prior to measurement, thus avoiding oxidation.

Magnetic susceptibility measurements were carried out on powders encapsulated within gelatin capsules and fixed with solidified melted wax. Measurements were carried out in the temperature interval 5–300 K using a Quantum Design superconducting quantum interference device (SQUID) with an applied field of 100 G.

III. RESULTS

A. XRD profiles

Figure 1 shows the XRD profiles for $EuCoO_3$ and $Ce_xEu_{1-x}CoO_3$ ($x = 0.05$, 0.10, 0.15, and 0.20) obtained from firing the adequate cobalticyanide metal complexes. As pointed out in Ref. 10, by the present preparation method the solid solution has only been obtained within the compositional range $x < 0.15$; at $x \geqslant 0.15$ the doped Ce ions partially precipitate as a second phase, i.e., CeO_2, as recognized by a diffraction peak at approximately $2\theta = 28°$.

The lattice constants, as extracted by means of the Rietveld method, are shown in Fig. 2 as a function of Ce-doping concentration x. The values are well represented by a linear relation against the concentration x. The cerium-doped solid solution with composition $x = 0.05$ was synthesized in this work. The lattice constants were computed to be $a = 53.838(2)$ nm, $b = 74.812(3)$ nm, and $c = 52.568(2)$ nm.

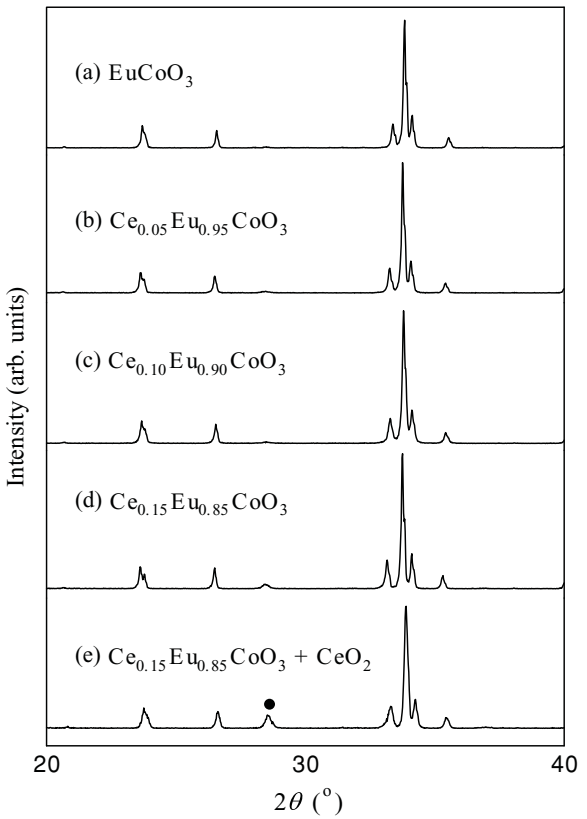

FIG. 1. XRD profiles of the residues obtained from firing $Ce_xEu_{1-x}[Co(CN)_6]6H_2O$ at 1473 K: (a) $x = 0$; (b) $x = 0.05$; (c) $x = 0.10$; (d) $x = 0.15$; (e) $x = 0.20$. The resultant products are specified in the legends within the figure. The diffraction peak arising from the presence of the CeO_2 impurity is labeled with •.

B. XAS spectra

Figure 3 shows the Ce L_3 XAS spectra for Ce compounds taken at room temperature. The spectrum for $Ce_{0.1}Eu_{0.9}CoO_3$ essentially resembles that of CeO_2. In contrast to this, the spectrum for $Ce_{0.1}Eu_{0.9}AlO_3$ resembles that of $Ce(NO_3)_3$. These results enable us to judge the Ce ions in $Ce_{0.1}Eu_{0.9}CoO_3$ and $Ce_{0.1}Eu_{0.9}AlO_3$ clearly as being in a tetravalent and a trivalent state, respectively, at room temperature.

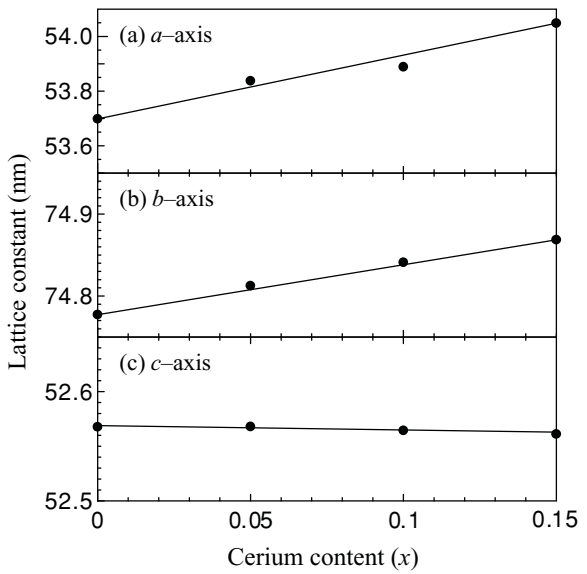

FIG. 2. Dependence of lattice constants on Ce-doping concentration for $Ce_xEu_{1-x}CoO_3$: (a) a axis; (b) b axis; (c) c axis.

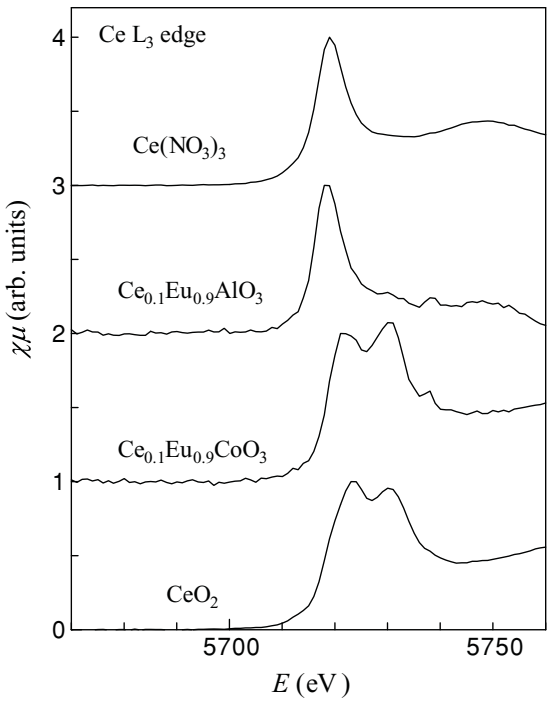

FIG. 3. Room-temperature Ce L_3 x-ray absorption edge spectra of $Ce_{0.1}Eu_{0.9}MO_3$ (M = Al, Co) and Ce^{3+} [$Ce(NO_3)_3$] and Ce^{4+} (CeO_2) reference materials. The ordinates of upper spectra are shifted upward each in order by 1.

Figures 4 and 5(a) give the Eu L_3 and Co K XAS spectra, respectively, for $Ce_xEu_{1-x}CoO_3$ ($x = 0$, 0.1); the dashed lines represent the results of $x = 0$, and a solid line in Fig. 4 and a dotted one in Fig. 5(a) represent the results of $x = 0.1$. The Eu L_3 absorption edge peak position of the trivalent Eu spectrum remains unchanged upon Ce doping, clearly indicating that the whole Eu ions are trivalent also in $Ce_{0.1}Eu_{0.9}CoO_3$. On the other hand, the Co K XAS spectra displayed in Fig. 5(a) differ subtly between the $EuCoO_3$ and Ce-doped samples. Because the doped Ce ions were seen to be tetravalent amid the trivalent Eu ions, one naturally expects this difference to stem from the existence of equivalent amounts of Co^{2+} ions, i.e., of localized doped electrons. To elucidate this expectation, the 90% weighted $EuCoO_3$ spectrum was subtracted from the $Ce_{0.1}Eu_{0.9}CoO_3$ spectrum; the difference spectrum is shown with a solid line in Fig. 5(b). In Fig. 5(c), this difference spectrum was enlarged by a factor of 10 and was displayed as a solid line along with the spectra for the reference materials CoO (a dotted line) and $EuCoO_3$ (a dashed line) symbolizing Co^{2+} and Co^{3+} valence states, respectively. From this comparison, it is seen that the difference spectrum features one peak and two humps whose positions and relative heights mimic well the CoO reference spectrum.[14] Indeed, the edge peak position coincides better with the spectrum of CoO than with that of $EuCoO_3$. This strongly suggests that this resultant spectrum stems from

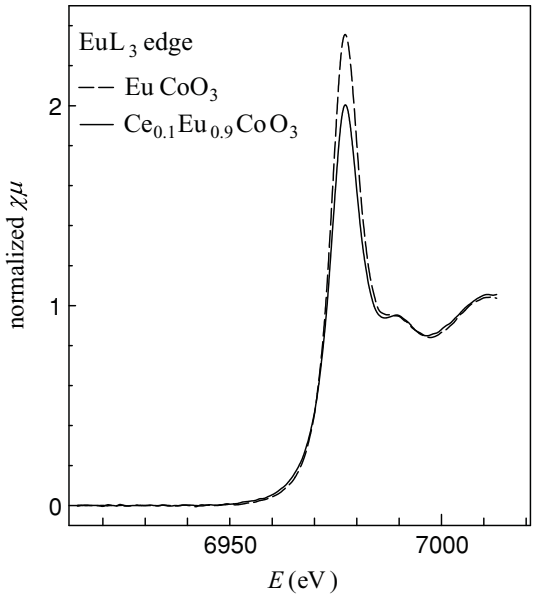

FIG. 4. Normalized room-temperature Eu L_3 x-ray absorption edge spectrum of $Ce_{0.1}Eu_{0.9}CoO_3$ (solid line) and $EuCoO_3$ (dashed line). The values were normalized by the one to which they converge at high post-edge x-ray energies.

the existence of Co^{2+} centers in $Ce_{0.1}Eu_{0.9}CoO_3$. Therefore, these results support the room-temperature description of the system as $Ce^{IV}_{0.1}Eu^{III}_{0.9}(Co^{II}_{0.1}Co^{III}_{0.9})O_3$, i.e., a localized scenario for the doped electrons.

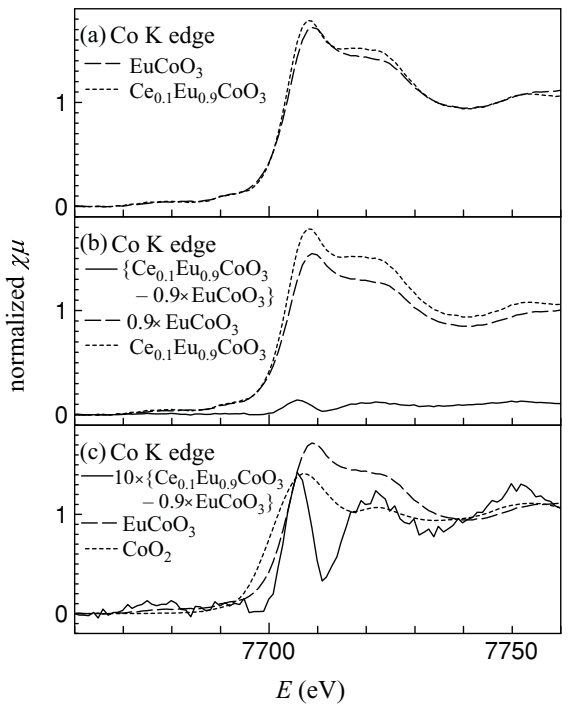

FIG. 5. Normalized room-temperature Co K x-ray absorption edge spectra: (a) $EuCoO_3$ (dashed line) and $Ce_{0.1}Eu_{0.9}CoO_3$ (dotted line); (b) 90% weighted $EuCoO_3$ (dashed line), $Ce_{0.1}Eu_{0.9}CoO_3$ (dotted line), and the difference spectrum between the two (solid line); (c), $EuCoO_3$ (dashed line), CoO (dotted line), and the difference spectrum in (b), multiplied by 10 (solid line).

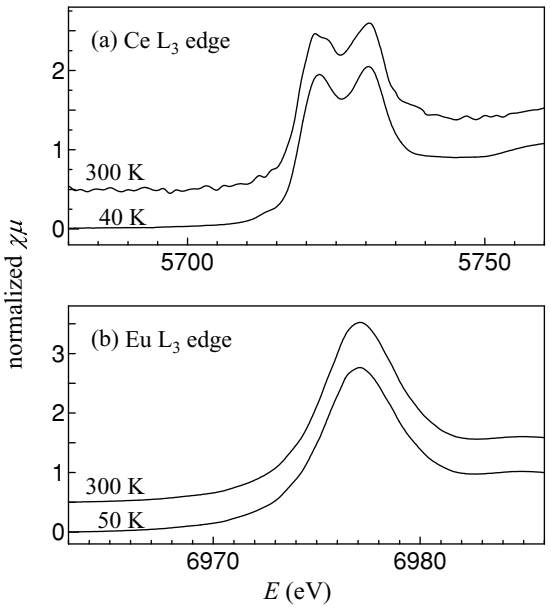

FIG. 6. Temperature dependence of normalized x-ray absorption spectrum for $Ce_{0.1}Eu_{0.9}CoO_3$: (a) Ce L_3 edge at 40 and 300 K; (b) Eu L_3 edge at 50 and 300 K. The ordinates of the respective upper spectra are shifted upward by 0.5.

Figure 6 shows the comparison between the Ce [see Fig. 6(a)] and Eu [see Fig. 6(b)] L_3 XAS spectra at 300 K and at 40 or 50 K for $Ce_{0.1}Eu_{0.9}CoO_3$; for clarity, the ordinate is shifted slightly upward for the spectrum at 300 K in both figures. Essentially no change in the XAS spectra with decreasing temperature was observed for either of the rare-earth elements, indicating that no valence change occurs with these elements.

Figure 7(a) shows the Co K XAS spectrum at 40 K for $Ce_{0.1}Eu_{0.9}CoO_3$ as a dotted line; the Co K XAS spectrum for $EuCoO_3$ at room temperature is also displayed with a dashed line for reference. Contrary to what was observed in the room-temperature XAS measurements, the Co K edge peak shape for $Ce_{0.1}Eu_{0.9}CoO_3$ at low temperature is essentially the same as the room temperature $EuCoO_3$ one. The spectra themselves appear to differ only in the pre-edge region; the intensity of a pre-edge broad peak in the $Ce_{0.1}Eu_{0.9}CoO_3$ spectrum is slightly weaker as compared with that in $EuCoO_3$ [see the inset of Fig. 7(a)]. This feature is essentially the same result obtained by Pinto *et al.*[6] for $Ce_{0.1}La_{0.9}CoO_3$ and indicates that the doped electrons are incorporated into the Co d bands. Figure 7(b) shows the difference between the low-temperature $Ce_{0.1}Eu_{0.9}CoO_3$ Co K XAS spectrum and the 90% weighted $EuCoO_3$ Co K XAS spectrum; the difference is shown as a solid line. Subsequently, the difference multiplied by a factor of 10 is displayed, along with the reference spectra for CoO (a dotted line) and $EuCoO_3$ (a dashed line), in Fig. 7(c). It is evident that the difference spectrum resembles that of $EuCoO_3$ instead of CoO, contrary to what was previously observed at room temperature as shown in Fig. 5(c). In this manner, the low-temperature XAS results are understood as best given by the electronic structure of $Ce^{IV}_{0.1}Eu^{III}_{0.9}Co^{2.9+}O_3$, i.e., by an itinerant-electron description.

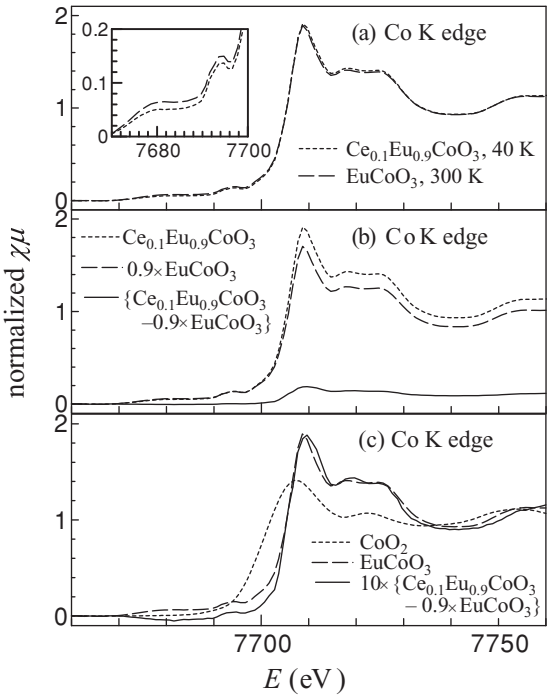

FIG. 7. Normalized room- and low-temperature Co K x-ray absorption edge spectra: (a) $EuCoO_3$ at 300 K (dashed line) and $Ce_{0.1}Eu_{0.9}CoO_3$ at 40 K (dotted line); (b) 90% weighted $EuCoO_3$ at 300 K (dashed line), $Ce_{0.1}Eu_{0.9}CoO_3$ at 40 K (dotted line) and the difference spectrum between the two (solid line); (c) $EuCoO_3$ (dashed line), CoO (dotted line), and the difference spectrum in (b), multiplied by 10 (solid line).

The results shown in Figs. 5(c) and 7(c) are simultaneously displayed in Fig. 8. The difference in the peak positions (as marked with dashed and dashed-dotted vertical lines) indicates the change in the electronic structure of Co ions in $Ce_{0.1}Eu_{0.9}CoO_3$ as ascribed to the temperature change.

C. Magnetic susceptibility

The molar magnetic susceptibility of the polycrystalline $EuCoO_3$ prepared by the thermal decomposition of the appropriate metallic complex was given in Ref. 10. There, the spectra below room temperature showed a fairly small deviation from the Eu^{3+} ion's theoretical Van Vleck paramagnetism, and it was claimed that the majority of Co^{3+} ions is in the LS state over the entire temperature range.[10] Baier *et al.* reported magnetic susceptibility data on single crystals of the system $Eu_xLa_{1-x}CoO_3$ ($x = 0 - 1$).[14] The magnetic susceptibility of $EuCoO_3$ was described as representing up to almost 400 K by the van Vleck susceptibility of Eu^{3+},[15] and it was indicated that the majority of Co^{3+} ions is in the LS state.

As stated above, the analysis of the XAS spectra reveals the presence of Co^{2+} centers, i.e., localized electrons, in $Ce_xEu_{1-x}CoO_3$ at room temperature. These Co^{2+} centers are understood to be magnetically active and, hence, they should contribute to the magnetic properties of $Ce_xEu_{1-x}CoO_3$. The magnetic susceptibility of $Ce_xEu_{1-x}CoO_3$ was thus analyzed, taking the presence of these paramagnetic Co^{2+} centers into consideration. The temperature dependence of the molar magnetic susceptibility $\chi_{m,Co^{2+}}$ associated with the paramagnetic

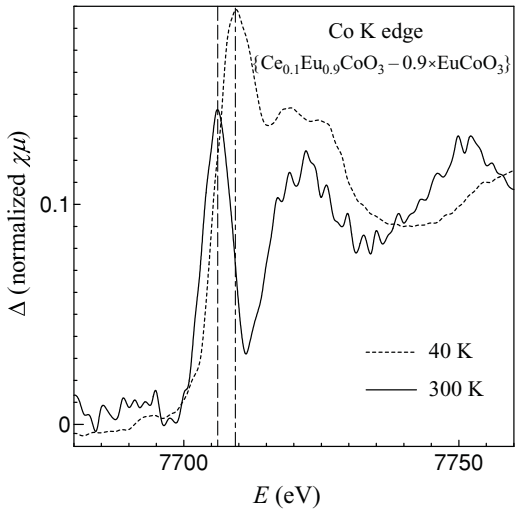

FIG. 8. Comparison of the two Co K edge spectra for $Ce_{0.1}Eu_{0.9}CoO_3$, represented as the differences between the spectra for $Ce_{0.1}Eu_{0.9}CoO_3$ and $0.9EuCoO_3$, derived in Fig. 5(b)) at room temperature (solid line) and in Fig. 7(b)) at 40 K (dotted line). The dashed and dashed-dotted vertical lines mark the energies at peak tops of the respective spectra and are guides to the eyes.

Co^{2+} centers is given in Fig. 9 for $Ce_xEu_{1-x}CoO_3$ ($x = 0.05$, 0.1, 0.15), where the solid, dotted, and dashed lines represent the results of $x = 0.05$, 0.1, and 0.15, respectively. The Co^{2+} molar magnetic contribution was extracted by eliminating the Eu^{3+} van Vleck contribution $\chi_{Eu^{3+}}$ according to the following equation:[16]

$$\chi_{m,Co^{2+}} = \frac{\chi_{obs} - (1-x)\chi_{Eu^{3+}}}{x}. \quad (1)$$

Diamagnetic corrections were calculated from Pascal's constants.[17]

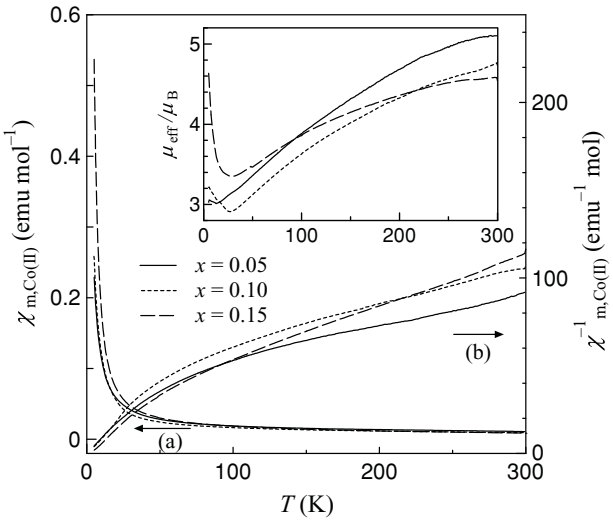

FIG. 9. Temperature dependence of (a) the resolved molar magnetic susceptibilities for Co^{2+} population within $Ce_xEu_{1-x}CoO_3$ [as determined according to Eq. (1)] and (b) their inverses for $x = 0.05$ (solid line), $x = 0.10$ (dotted line), and $x = 0.15$ (dashed line). The inset shows the effective magnetic moments calculated based on the Curie equation.

Figure 9 also shows the inverse of $\chi_{m,\mathrm{Co}^{2+}}$, the scale of which is written on the right-hand-side ordinate. It is noticed from the nonlinear behavior of the inverse magnetic susceptibility that the magnetic behavior follows no simple Curie relation. The inset of Fig. 9 shows the associated effective magnetic moment μ_{eff} determined from the Curie equation. The μ_{eff} at room temperature reaches values as high as $5.1\mu_{\mathrm{B}}$ when $x = 0.05$. The value surpasses the (localized-electron) spin-only value for high-spin Co^{2+}, i.e., $3.87\mu_{\mathrm{B}}$ $(= [4S(S+1)]^{1/2}$ with $S = 3/2)$. Many research groups attribute this kind of anomalous behavior to the strong orbital contribution to the magnetic moment.[18,19] Indeed, the μ_{eff} value of $5.1\mu_{\mathrm{B}}$ approaches the value expected when both the spin momentum and the orbital momentum contribute independently, i.e., $5.20\mu_{\mathrm{B}}$ $(= [L(L+1) + 4S(S+1)]^{1/2}$ with $L = 3$ and $S = 3/2)$. These facts suggest the existence of orbital contribution to the magnetic susceptibility. Evidence for orbital contribution to the magnetic properties has been found also in perovskite systems with Co^{2+} centers such as $LaMn_{0.5}Co_{0.5}O_3$.[18]

As the Ce-doping concentration is increased from $x = 0.05$ toward $x = 0.15$, the room-temperature effective magnetic moment μ_{eff} decreases proportionally, as shown in the inset of Fig. 9. The temperature dependence of μ_{eff} for $x = 0.10$ resembles qualitatively that of $x = 0.05$, although it is quantitatively smaller, and both data run parallel to each other. As $T \to 0$ K, a sudden rise in μ_{eff} starts to set in for $x = 0.10$ and 0.15: This quick increase of μ_{eff} clearly dominates the low-temperature magnetic response. This increase stems from the presence of ferromagnetic interactions.[20] The Curie-Weiss law may be employed in an attempt to characterize this ferromagnetism by analyzing the linearity of the low-temperature end region of $\chi^{-1}_{m,\mathrm{Co}^{2+}}$. The analysis yielded $T_c(x = 0.10) = 1.8$ K and $T_c(x = 0.15) = 3.0$ K.

IV. DISCUSSION

A. Crossover from low-temperature itinerant-electron to high-temperature localized-electron behaviors

The present results regarding the valence states of the ionic species in $Ce_xEu_{1-x}CoO_3$ are in disagreement with the conclusion from the previous work of Umemoto *et al.*,[10] and instead support the room-temperature description of the system as $Ce^{IV}_{0.1}Eu^{III}_{0.9}(Co^{II}_{0.1}Co^{III}_{0.9})O_3$. According to the analysis presented above, the doped Ce ions are tetravalent, and the partial loss of electrons by the doping at A sites is compensated for by the reduction of the same amount of the B-site cobalt ions from trivalent to divalent states. Actually, evidence for the combination Ce^{4+}:Co^{2+} may also be inferred by noticing that the complete substitution of Co by Al in $Ce_{0.1}Eu_{0.9}MO_3$ (M = Al, Co) induces a change in the valence state of Ce toward a trivalent one as shown in Fig. 4. However, opposed to this room-temperature localized-electron description, our low-temperature XAS measurements failed to identify Co^{2+} centers, indicating the system to be best described as $Ce^{IV}_{0.1}Eu^{III}_{0.9}Co^{2.9+}O_3$ at low temperatures. Thus, we have concluded that a crossover from localized-electron to itinerant-electron behavior occurs as the temperature is decreased (see Fig. 8).

The change of behavior of the electron localized on a Co ion to that itinerant over all Co ions with temperature should naturally have repercussions in the magnetic properties of the system. In order to elucidate these effects, it is illustrative to compare the observed magnetic susceptibility with the magnetic response expected for Co^{2+}, i.e., when the electron is localized in the entire temperature range. The magnetic properties of six-coordinated high-spin Co^{2+} compounds are in general more complex than those containing other transition metals, which may be treated with a spin-only formalism; this is owing to the presence of a strong orbital contribution.[20–23] The magnetic response for a high-spin Co^{2+} ion in a O_h environment is given as a function of the crystal-field strength, i.e., the ratio of the crystal-field parameter Dq to the Racah parameter B, and two other parameters: the spin-orbit coupling parameter λ and the orbital reduction factor κ. These last two parameters account for covalency effects related to the metal-ligand bonds and for the free Co^{2+} ion case are known to be $\lambda_0 = 172$ cm^{-1} (Ref. 22) and $\kappa_{\mathrm{free\ ion}} = 0.93$.[22] In $EuCoO_3$, Dq is of the order of 0.1 eV (806 cm^{-1}) (Ref. 24) and B is ~780 cm^{-1} for Co^{2+} in CoO,[25] thus suggesting a weak field for Co^{2+} in $EuCoO_3$.[26] However, should the ligands' symmetry be distorted from the ideal octahedral one, such as to lower symmetries as D_{4h} or D_{2h}, parameters designating these axial or rhombic distortions should also be taken into consideration to account for the splitting of symmetry terms.[23] From the present results, the type of local distortion and, consequently, the symmetry of the octahedra surrounding the Co^{2+} ions in the room-temperature $Ce_xEu_{1-x}CoO_3$ are unclear. In order to simulate the most probable Co^{2+} magnetic response, we fitted the high-temperature magnetic susceptibility data for $Ce_{0.05}Eu_{0.95}CoO_3$ by setting a weak field ($A = 1.5$; see Refs. 20 or 26 for the meaning of this parameter) and introducing an axial distortion parameter Δ to account for the possible octahedral distortions according to the magnetic equations provided by Ref. 20. Fits were performed for various values of κ, departing from the free-ion value, in order to take into account potential covalent effects and/or departures from the assumed weak field. The spin-coupling parameter was kept fixed at the free-ion value λ_0. Our results show that reproduction of the high-temperature magnetic data was only possible in the range $\kappa \geqslant 0.90$, and for this condition $|\Delta| \leqslant 180$ cm^{-1} was obtained. The results are given in Fig. 10, expressed as $\chi_{m,\mathrm{Co(II)}}T$. From this figure, it is seen that the decrease of $\chi_{m,\mathrm{Co}^{2+}}T$ with decreasing temperature is quicker for the experimental data than for the theoretical curves, and the deviation from the theoretical curve is considerable. The discrepancy between the data and the theoretical curves means that the magnetic properties of electron-doped Co ions cannot be expressed by the parameters fixed over the entire temperature range; namely, the electronic structure of the relevant Co ions cannot be expressed simply by the presence of Co^{2+} ions. The result is consistent with the one of the XAS spectra for electron-doped Co ions, that the electronic structure crosses over from a localized electron as Co^{2+} at room temperature to an itinerant electron as Co^{3+} at low temperatures.

The hole-doped cobaltates $Sr_xR_{1-x}CoO_3$ are known to show low-temperature ferromagnetism for $x > 0.125$, and

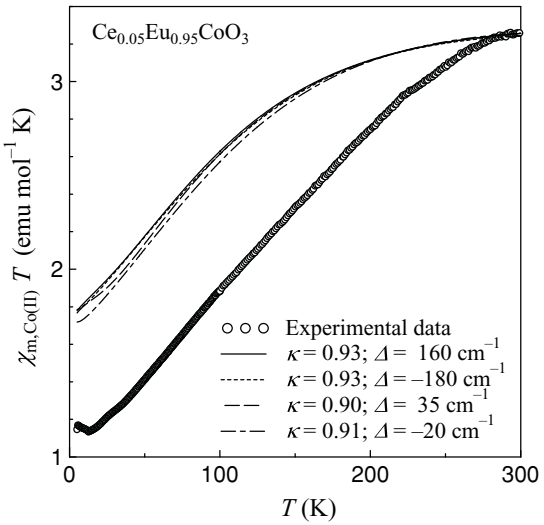

FIG. 10. $\chi_{m,\mathrm{Co(II)}}T$ plots of experimental data for $Ce_{0.05}Eu_{0.95}CoO_3$ (open circles) and theoretical curve (solid line) for divalent cobalt in an O_h field. The magnetic equation from Ref. 20 was used for the theoretical curve calculation with $\lambda = 172$ cm^{-1}, $A = 1.5$, and κ and Δ are parameters assuming the different sets of values written inside the figure.

this has been understood in terms of an itinerant-electron model, supporting the existence of itinerant-electron ferromagnetism.[27] In these hole-doped counterparts, the *d*-electron's itinerant behavior is conceived to hold both above and below T_c with μ_{eff} falling in between 1.3 and 2.8.[27] In accordance to the localized–itinerant-electron crossover as depicted by the present XAS measurements on $Ce_{0.1}Eu_{0.9}CoO_3$, a corresponding crossover from temperature-dependent Co^{2+} paramagnetic behavior to temperature-independent Pauli paramagnetism was expected to occur in the magnetic regime for the most dilute Ce-doped compound, i.e., $x = 0.05$. However, as seen from Fig. 10, no discontinuities in $\chi_{m,\mathrm{Co(II)}}T$ occur down to the lowest temperatures; the small low-temperature kink is attributed to the presence of small amounts of magnetic impurities such as grain-boundary and/or surface ions. Nevertheless, Fig. 10 shows that $\chi_{m,\mathrm{Co}^{2+}}T$ tends to go toward the value of ~1.0 emu mol^{-1} K as $T \to 0$ K, a value that is much smaller than the expected limit value of 1.7–1.5 emu mol^{-1} K as $T \to 0$ K for Co^{2+} in an O_h symmetry.[20] It is further noted that the value of 1.0 emu mol^{-1} K ($\mu_{\mathrm{eff}} = 2.8\mu_{\mathrm{B}}$) is comparable to μ_{eff} found in the hole-doped cobaltates,[27] suggesting the behavior of the low-temperature magnetic susceptibility to result from itinerant electrons.

B. Competition between antiferromagnetic localized electrons and ferromagnetic itinerant electrons

The decrease of the room-temperature effective magnetic moment μ_{eff} in $Ce_xEu_{1-x}CoO_3$ can be attributed to the presence of a Co^{II}-O-Co^{II} antiferromagnetic coupling, which becomes more probable with increasing Ce concentration. As the temperature is lowered, the localized-to-itinerant crossover will dissolve these antiferromagnetically coupled regions, allowing itinerant ferromagnetism. Accordingly, it can be expected that at high temperatures (i.e., room temperature) μ_{eff} will be inversely proportional to the doping concentration x, whereas at low temperatures it will be proportional. Hence, a comparison of magnetic data of samples with different doping concentrations should reveal this inversion. From the inset of Fig. 9, the inversion of the relation $\mu_{\mathrm{eff}}(x = 0.15) < \mu_{\mathrm{eff}}(x = 0.10)$ at room temperature to $\mu_{\mathrm{eff}}(x = 0.15) > \mu_{\mathrm{eff}}(x = 0.10)$ is observed to occur already at ~200 K. Similarly, this inversion takes place at ~100 K when the samples with $x = 0.05$ and 0.15 are compared. However, the answer as to why a similar feature is not identified when considering the $x = 0.05$ and 0.10 samples is unclear at the present moment.

Fuchs *et al.* have reported an increase of room temperature μ_{eff} with x for $Ce_xLa_{1-x}CoO_3$ and argued that electron doping increases the stability of the IS Co^{3+} state, thereby increasing the number of magnetic species.[7] This differs from the dependence of room-temperature μ_{eff} on x observed for $Ce_xEu_{1-x}CoO_3$ presented here. Lack of an inversely proportional relation between μ_{eff} and x suggests antiferromagnetic interactions to be apparently nonexistent in room-temperature $Ce_xLa_{1-x}CoO_3$. This fact might be an indication that a similar localized-to-itinerant crossover phenomenon is not inherent in $Ce_xLa_{1-x}CoO_3$. Nevertheless, it is possible that the influence of excited cobalt spin states, i.e., IS or HS, present in room-temperature $Ce_xLa_{1-x}CoO_3$ but apparently not in $Ce_xEu_{1-x}CoO_3$, may suppress antiferromagnetic interactions between potential Co^{2+} centers within $Ce_xLa_{1-x}CoO_3$. Another possibility is that localized electrons within $Ce_xLa_{1-x}CoO_3$, i.e., Co^{2+}, might only occur at temperatures higher than room temperature, implying the potential dependence of the localized-to-itinerant crossover temperature range on the rare-earth radii. Further experimental evidence is required to address the veracity of these possibilities.

V. CONCLUSION

The valence states in the solid solution $Ce_xEu_{1-x}CoO_3$ ($x \leqslant 0.15$) were elucidated by means of XAS spectroscopy. As opposed to what was previously reported,[10] the present experiments clearly showed that the Ce is tetravalent and the Eu is trivalent in the entire temperature range below 300 K, confirming the electron-doped nature of $Ce_xR_{1-x}CoO_3$ compounds. Furthermore, the presence of a crossover phenomenon from the low-temperature itinerant-electron to high-temperature localized-electron behaviors on the partial Co ions was identified through elucidating the presence or absence of Co^{2+} population as observed by the XAS measurements. This itinerant-to-localized electron crossover differs from the well-known crossover from localized-to-itinerant electron behavior in pure $RCoO_3$, which is associated with a change of spin state of the cobalt ions. The temperature dependence of the magnetic susceptibility of $Ce_xEu_{1-x}CoO_3$ ($x \leqslant 0.15$) was understood to be potentially consistent with this itinerant-to-localized electron crossover deduced from the XAS results.

This itinerant-to-localized electron crossover is expected not to be peculiar to the system $Ce_xEu_{1-x}CoO_3$ but to be universal in electron-doped rare-earth cobaltates. However,

this crossover may be obscured in the compounds that acquire a considerable population of IS or HS Co^{3+} before the crossover can occur, such as the $RCoO_3$ members with the lighter rare-earth elements. Furthermore, the possibility that a similar phenomenon occurs, for example, in the perovskite manganites is of great interest. In order to elucidate if this itinerant-to-localized electron crossover is present in other $RCoO_3$ members, further investigations are needed to fully understand the energetics and the driving forces behind this phenomenon.

ACKNOWLEDGMENTS

The authors are grateful to Katsumi Suda of the Center for Advanced Materials Analysis at the Tokyo Institute of Technology for help with room-temperature XAS measurements. The XAS measurements at the Photon Factory were performed under the approval of the Photon Factory Advisory Committee (proposal No. 2008P106). The authors thank Kiyofumi Nitta of KEK for help with low-temperature XAS measurements.

[1] J. B. Goodenough, Prog. Solid State Chem. **5**, 145 (1972).
[2] G. Thornton, F. C. Morrison, S. Partington, B.C. Tofield, and D. E. Williams, J. Phys. C **21**, 2871 (1988).
[3] C. N. R. Rao, M. M. Seikh, and C. Narayana, Top Curr. Chem. **234**, 1 (2004).
[4] M. A. Señarís-Rodríguez and L. B. Goodenough, J. Solid State Chem. **116**, 224 (1995).
[5] M.A. Señarís-Rodríguez and L. B. Goodenough, J. Solid State Chem. **118**, 323 (1995).
[6] C. Pinta, D. Fuchs, E. Pellegrin, P. Adelmann, S. Mangold, and S. Schuppler, J. Low Temp. Phys. **147**, 421 (2007).
[7] D. Fuchs, P. Schweiss, P. Adelmann, T. Schwarz, and R. Schneider, Phys. Rev. B **72**, 014466 (2005).
[8] C. Mitra, P. Raychaudhuri, J. John, S. K. Dhar, A. K. Nigam, and R. Pinto, J. Appl. Phys. **89**, 524 (2001).
[9] Q. Zhang, X. Huang, W. Zhang, and A. Hu, J. Appl. Phys. **95**, 6822 (2004).
[10] K. Umemoto, Y. Seto, and Y. Masuda, Thermochim. Acta **431**, 117 (2005).
[11] S. Nakayama, M. Okazaki, Y. L. Aung, and M. Sakamoto, Solid State Ion. **158**, 133 (2003).
[12] M. Nomura and A. Koyama, KEK Report No. 95-15, 1996 (unpublished).
[13] B. Ravel and M. Newville, J. Synchrotron Rad. **12**, 537 (2005); M. Newville, *ibid.* **8**, 322 (2001).
[14] The normalized Co XAS spectrum intensities for $Ce_{0.1}Eu_{0.9}CoO_{3+\delta}$:$Co^{2+}$ and CoO could be approximately well matched by multiplying the former by a factor of 10 after subtraction of the Co^{3+} contribution [see Fig. 6(c)]. This in turn suggests the Co^{2+} population is nearly 10% within $Ce_{0.1}Eu_{0.9}CoO_3$, substantiating the idea that $\delta \approx 0$.
[15] J. Baier, S. Jodlauk, M. Kriener, A. Reichl, C. Zobel, H. Kierspel, A. Freimuth, and T. Lorenz, Phys. Rev. B **71**, 014443 (2005).
[16] J. H. Van Vleck, *The Theory of Electric and Magnetic Susceptibilities* (Oxford University Press, Oxford, 1932).
[17] G. A. Bain and J. F. Berry, J. Chem. Educ. **85**, 532 (2008).
[18] T. Burnus, Z. Hu, H. H. Hsieh, V. L. J. Joly, P. A. Joy, M. W. Haverkort, H. Wu, A. Tanaka, H.-J. Lin, C. T. Chen, and L. H. Tjeng, Phys. Rev. B **77**, 125124 (2008).
[19] G. Ghiringhelli, L. H. Tjeng, A. Tanaka, O. Tjernberg, T. Mizokawa, J. L. de Boer, and N. B. Brookes, Phys. Rev. B **66**, 075101 (2002).
[20] F. Lloret, M. Julve, J. Cano, R. Ruiz-García, and E. Pardo, Inorg. Chim. Acta **361**, 3432 (2008).
[21] H. Sakiyama, Inorg. Chim. Acta **359**, 2097 (2006).
[22] H. Sakiyama, R. Ito, H. Kumagai, K. Inoue, M. Sakamoto, Y. Nishida, and M. Yamasaki, Eur. J. Inorg. Chem. 2027 (2001).
[23] A. Palii, B. Tsukerblat, J. M. Clemente-Juan, and E. Coronado, Inter. Rev. Phys. Chem. **29** (), 135 (2010).
[24] Z. Hu, Hua Wu, M. W. Haverkort, H. H. Hsieh, H.-J. Lin, T. Lorenz, J. Baier, A. Reichl, I. Bonn, C. Felser, A. Tanaka, C. T. Chen, and L. H. Tjeng, Phys. Rev. Lett. **92**, 207402 (2004).
[25] A. M. Hennel, J. Phys. C **11**, L389 (1978).
[26] The strength of the field may be expressed through the A parameter, i.e., $A = \frac{\frac{3}{2}-c^2}{1+c^2}c = 0.75 + 1.875\frac{B}{Dq} - 1.25[1 + 1.8\frac{B}{Dq} + 2.25(\frac{B}{Dq})^2]^{1/2}$, and its values for the weak and strong field situations are $A = 3/2$ and $A = 1$, respectively (Ref. 20). Insertion of $Dq = 806$ cm^{-1} from Ref. 24 and $B = 780$ cm^{-1} from Ref. 25 yields $A = 1.41$, suggesting that the crystal field is more inclined toward a weak field rather than a strong field.
[27] C. N. R. Rao, O. M. Parkash, D. Bahadur, P. Ganguly, and S. Nagabhushana, J. Solid State Chem. **22**, 353 (1977).